This is the Pre-Published Version.

C. Xiong, X. Huang (2021) *Numerical Modeling of Flame Shedding and Extinction behind a Falling Thermoplastic Drip,* **Flow, Turbulence and Combustion**. doi: 10.1007/s10494-021-00250-5

Numerical Modeling of Flame Shedding and Extinction behind a Falling Thermoplastic Drip

Caiyi Xiong[1,2] and Xinyan Huang[1,*]

[1]*Research Centre for Fire Safety Engineering, The Hong Kong Polytechnic University, Hong Kong*

[2]*The Hong Kong Polytechnic University Shenzhen Research Institute, Shenzhen, China*

*Corresponding Author: xy.huang@polyu.edu.hk

Abstract

The dripping of molten thermoplastics is a widely observed phenomenon in cable and façade fire, where the large drips can often carry a blue chain flame during the free fall to ignite other flammable materials and escalate the fire hazard. This work simulated the flame evolution behind a falling thermoplastic drip with the DNS model and finite-rate flame chemistry. The accelerated free-fall of drip was modeled by fixing the position of drip, increasing the upward airflow, and setting a fuel jet on the top of the drip. Modeling reproduces the dripping flame and reveals the flame shedding to be a combination of a lifted flame and a vortex street, where the lifted flame caused by the gravity acceleration of drip is identified as the critical factor that governs the shedding formation. As the diameter of drip decreases, the falling drip becomes difficult in forming a stable shedding structure in the wake region, so that the dripping extinction occurs due to the dilution and cooling of airflow, agreeing well with the experimental observation. This work reveals the underlying mechanism of stabilizing the dripping flame and helps evaluate the fire risk and hazard of dripping phenomena.

Keywords: Dripping flame; DNS; Flame shedding; Extinction; Moving fuel

1. Introduction

The phenomenon of dripping frequently occurs in electrical wire fires [1–5] and building façade fires [6–8] (Fig. 1a). The burning of thermoplastic material can melt, flow, and drip under the combined effect of surface tension and gravity. Once detached from the parent fuel, molten drips often carry a flame during the free fall, i.e., the dripping flame, and show the potential to ignite the nearby combustibles. As the flame attached to the drip acts as the pilot and heat source for dripping ignition, whether the flame can stably attach to the falling drip plays a critical role in the risk and hazard degree of dripping fire [1]. Thus, it is of both scientific interest and practical importance to study the dynamics of dripping flame and understand its extinction [9].

In the literature, dripping was generated by burning polymer slabs (e.g., the UL94 test [8, 10]) and wire insulations on metal tubes [1, 5, 11, 12] (Fig. 1b). The dripping ignitability correlates positively with both the drip size and dripping frequency [13], which are controlled by the material and external heating conditions [8, 10]. Several experiments explored the formation mechanism of thermoplastic drips in the wire fire under various wire configuration, oxygen concentration, and gravity levels [3, 14–16], while other researchers numerically modeled the melting, flow, and detachment of drips [2, 17, 18]. However, few lights of research have been shed on the fire hazard of dripping flame and the critical conditions of flame stabilization on the drip that continuously accelerates during the free fall. It can be

expected that the acceleration of drip can lead to a relative motion between the drip and flame, which affects the stability of dripping flame.

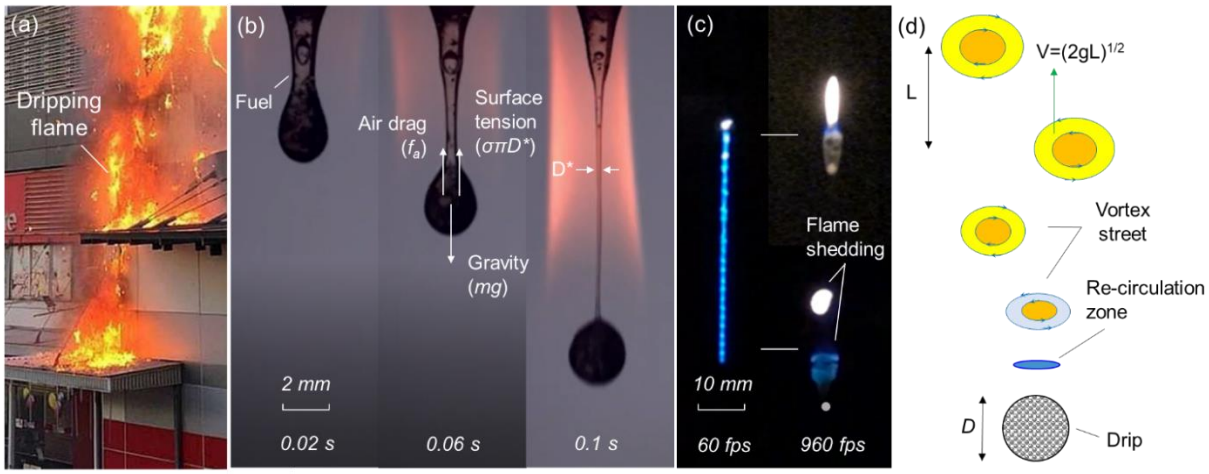

Fig. 1. (a) Dripping in façade fire, (b) the generation of a 2-mm polymer drip (Video S1), (c) dripping flame at 60 fps (blue chain flame, Video S2) and 960 fps (flame shedding, Video S3), and (d) possible vortex shedding behind drip.

In our previous work [1], the dripping flame was experimentally observed as a blue chain flame due to the persistence of vision (Fig. 1c), and the formation of dripping flame was hypothesized as a continuous ignition of the von Kármán vortex street (Fig. 1d), namely, the *flame shedding*. Such a shedding process was stable in the re-circulation zone of drip, even when it reached the terminal velocity of about 5 m/s. In addition, drips with a diameter smaller than 2 mm were found not able to hold a flame during the free fall, but the reason is still unclear. Considering the fast motion and tiny size of drip [1], it is very challenging in experiment to visually capture the detailed behaviors of dripping flame and explore the critical conditions for a drip to stabilize the flame. As the falling drip evolves in a complex and transient manner, it is different from the porous spherical gas burner in the constant upward flow [19, 20] where flame shedding was not observed between a stable wake flame and blow-off [21, 22]. Therefore, numerical simulation can be more effective in yielding insights into the evolution and dynamics of dripping flame.

As a summary, this study aims to develop a numerical model to reproduce the evolution of dripping flame, including the initial ignition and the subsequent transition from the envelope flame to wake flame, and then, to flame shedding, and explore the critical conditions of extinction. Boundary conditions are carefully set to mimic the real dripping process. Critical parameters for triggering flame shedding and extinction are explored in detail.

2. Numerical model

2.1. Geometric set-up

This study uses the Fire Dynamics Simulator (FDS, version 6.6.0) to establish the model and its DNS solver to calculate the finite-rate flame chemistry, which is analogous to the existing study [23]. Considering that FDS is a rectangular Cartesian solver, a 2-D domain with a size of 48 mm × 70 mm is established to easily build a circular geometry (Fig. 2a) and save computational cost. A planar Cartesian coordinate (x, y) is used to show the geometric position, where x and y stand for the horizontal and

vertical directions. The convergence study suggests that a uniform grid with the spatial resolution of Δl = 0.3 mm or smaller can resolve the flame with the 1-step finite-rate chemistry. To ensure the computational accuracy, a mesh with the resolution of Δl = 0.1 mm is adopted with 480 transverse nodes from x = -24 to 24 mm, and 700 streamwise nodes from y = -10 to 60 mm, leading to a final node number of 3.36×10^5.

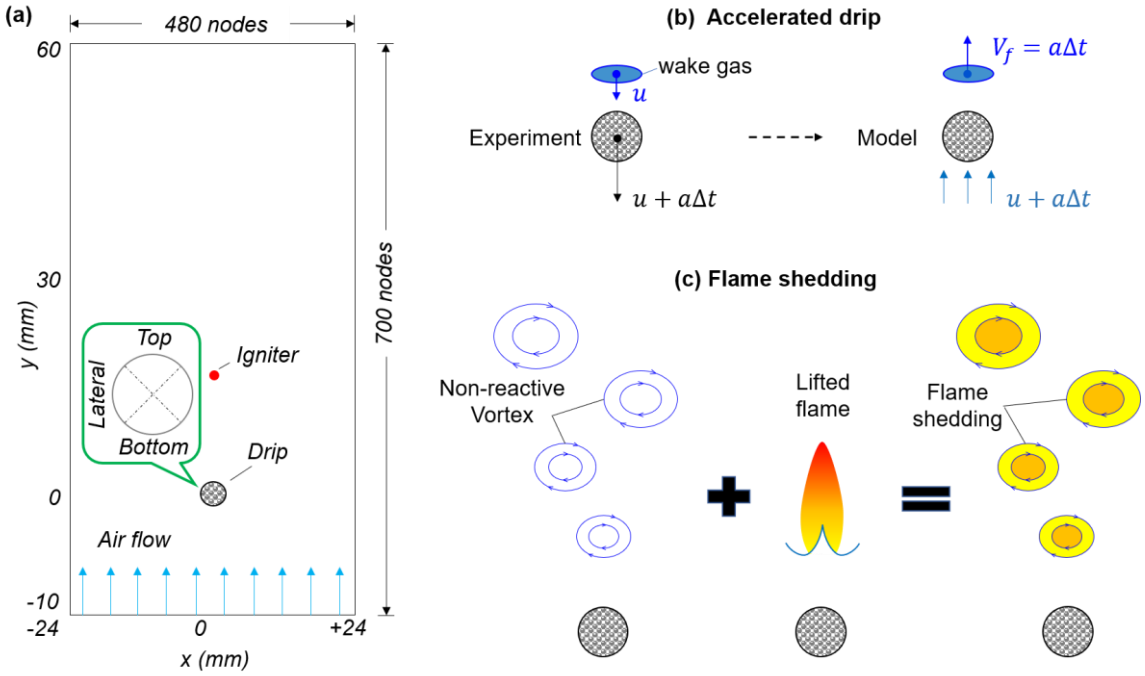

Fig. 2. Schematics of (a) computational domain, (b) drip acceleration, and (c) flame shedding.

A collapsing circular drip with the diameter ranging from 1 to 5 mm is used, referring to the drip size in the experiment (Figs. 1b-c) [13]. Because the falling polymer drips can only have a short lifetime (~ 1 s) [1], the drip sizes are kept constant during simulation. Moreover, several rectangles with a thickness of 0.1 mm are employed to approximate a circular geometry. In the model, the drip center coincides with the coordinate origin, and this configuration is the same as that used in our previous work [1]. The upgrade in this work is the use of 1-step finite-rate flame chemistry for the pyrolysis gases from the hot drip and the simulation of dripping flame. Parameters for the 1-step polymer flame chemistry include the pre-exponential factor A = 1.2×10^{16} mol/cm^3-s, the activation energy E_a = 100 kJ/mol, and the combustion heat Δh = 40 MJ/kg [23]. The temperature-related viscosity and diffusivity of ethylene are imposed on the fuel gas, which produces a Schmidt (Sc) number larger than 1 and is essential for stabilizing the flame [24, 25].

2.2. The domain boundary

The computational domain is bounded by four boundaries, including the bottom inflow boundary and other three open boundaries. To mimic the accelerated fall of a burning drip, the position of drip is fixed, and the bottom airflow (V_a) is increased referring to the measured speed of drip from experiment [1]. For example, a 2-mm falling drip can reach a terminal velocity of 4 m/s within 0.7 s in balance with the air friction [1], so its variation $V_a(t)$ is simplified as a linear profile in Fig. 3(a), where the fall starts from 2.0 s and reaches the terminal velocity at 2.7 s, resulting in a Reynolds number of Re = 504 (see

in Appendix). To keep a continuous combustion reaction, the side boundary must be transparent to the ambient flow. Thus, ambient conditions (25 ℃, 1 atm) are imposed on the two sides (Fig. 2a), and the horizontal velocities are treated naturally as the solutions from the governing equations to allow for continuous air entrainment. For the outflow boundary, it may generate wave reflection when the hot gas flows across it and affect the results. As suggested by the FDS user guide [26], ambient conditions are imposed at the position y = 100 mm where the hot gas from the largest 5-mm drip can be cooled by the bottom inflow to the room temperature. The computational results in the region higher than y = 60 mm are out of importance and therefore not used in the analysis.

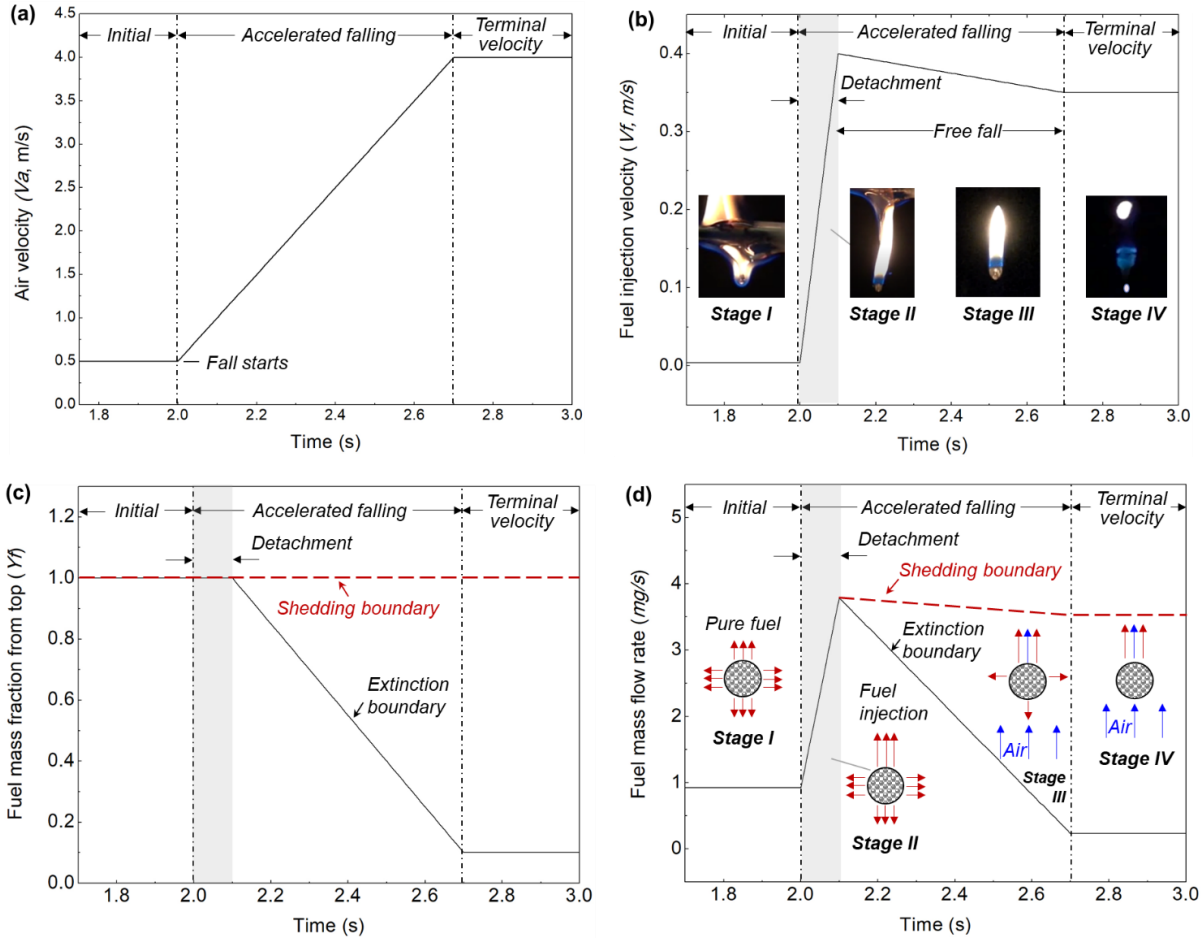

Fig. 3. Time evolutions of (a) upward airflow velocity, (b) the fuel injection velocity, following the observed dripping flame structures at different stages, (c) fuel mass fraction in the top stream, and (d) overall fuel mass rate by a 2-mm drip, where red arrow denotes fuel stream and blue arrow denotes air gas.

To pilot the flame, a hot igniter with a peak temperature of 1400 ℃ is placed in a single mesh that is 10 mm above the drip center and lasts for 0.7 s. Afterward, the igniter is removed, and the flame is required to stabilize itself under a constant bottom airflow of V_a = 0.5 m/s before the fall starts (t = 2.0 s, see Fig. 3a). This stage simulates the burning drip sustained on the parent fuel under the flame-induced buoyant flow (Stage I in Fig. 1b). The initial computational domain is set to have an ambient temperature of 25 ℃ and pressure of 1 atm. The simulation time advances evenly at a short step of 1 ms for chemical restraint. For modeling the dripping process of 8.0 s, each case requires nearly 10 days of the CPU-time by an MPI implementation with 13 threads.

2.3. The drip boundary

In a moving frame based on the drip, the dripping flame under the upward airflow can be seen as a bluff-body stabilized flame [27, 28]. It was known that solely introducing combustion reaction into a bluff-body flow would increase the baroclinic torque and reduce the vorticity, so as to prevent the occurrence of vortex shedding [29]. Also, the flame shedding was not found in past experiments with spherical burners [19, 20], which means that solely increasing the bottom airflow would not trigger flame shedding. The close examination of the accelerated falling process in experiment [1] indicates that an *acceleration-induced fuel injection velocity* (V_f) should be set on the top surface of the drip during the fall. There are two reasons for setting this velocity boundary: (1) due to the acceleration of drip, there is a relative velocity between the drip and the fuel stream behind (Fig. 2b), and (2) the flame shedding is similar to a lifted jet flame (Fig. 1c).

The variation of V_f in the model is set to be consistent with the real dripping behavior. Reexamining the formation of a 2-mm drip from the burning polyethylene (PE) wire in Fig. 1(b). Initially, the drip is suspended on the parent fuel since its gravity (mg) equals to its surface tension force ($\sigma\pi D^*$). As heated by the flame, the surface tension of drip decreases, so that gravity drags the drip downward where the net force on drip is

$$F_{net} = mg - \sigma\pi D^* - f_a = ma \tag{1}$$

where D^* is the diameter of the drip tail and f_a is the air friction which increases with dripping velocity. Thus, at the moment of detachment (Δt = 0.1 s in Fig. 1b) or the start of fall, f_a is small under a low velocity, and the drip tail is rapidly burnout ($D^* \to 0$), so that the acceleration of drip (a) is tending to its peak g. To mimic such a detaching process with the intensive burning of drip tail in the model, the acceleration-induced fuel injection velocity ($V_f \approx a\Delta t$) is increased to a peak value within 0.1 s, whose value is given by the von Kármán model [30] in the Appendix. Once the drip starts to fall, V_f is set to decay slowly because of the increasing in air friction, as shown in Fig. 3(b), and this decay needs to meet the mass conservation of the fuel stream discussed below.

2.4. The extinction parameters

There are two possible causes for flame extinction in small drips (D < 2 mm) in the experiment [1],

(1) Flame instability: the dripping flame was found not be able to catch up with small drips during the free fall [1], which leads to the fuel dilution by air and invites extinction; and
(2) Cooling effect: smaller drip experiences larger convective cooling from air during the fall, but the convective heating from flame may also increase.

In either case, the mass flow rate of the fuel gas released from hop drip can be defined as the factor that pays major contribution to the dripping extinction. In Figs. 3(c-d), different arrows were used to show the fuel stream or airflow at different dripping stages. For instance, a 2-mm drip is initially assumed to release pure ethylene gas at a fixed temperature of 400 °C (i.e., the pyrolysis point of polyethylene) with a constant mass rate of $\dot{m}$ = 0.92 mg/s. This value is given by the B-number (Spalding mass transfer number) of the stationary burning polymer [31, 32] and is far away from its extinction limit. As this drip develops to the detachment stage, a sudden increase in flame intensity by the burning of drip tail (Fig. 1b) is performed by a sharp increase in the fuel mass rate, which follows the variation of the fuel injection velocity (V_f) and is given by $\rho V_f S_{top}$. Here ρ = 1.83 kg/m^3 is the

density of ethylene gas and S_{top} = 3.14 mm^2 denotes the top surface area of a 2-mm drip (Fig. 2a, one quarter of the whole spherical area).

Once the dripping starts, the abovementioned two causes for flame extinction start to work. As the drip accelerates to fall, the fuel stream released by drip starts to mix with environmental air due to entrainment, represented by the decreasing fuel mass fraction Y_f from drip, seen in Fig. 3(c). Besides, to mimic the convective cooling during free fall, the fuel amount released from the lateral and bottom sides of drip is gradually decreased to zero. As a result, there is a whole decline of the fuel mass flow rate by drip during the accelerated falling stage in Fig. 3(d) and, eventually, only the drip top surface, which is continuously heated by the dripping flame above, can produce fuel gas at the terminal stage. To ensure the conservation of mass, the fuel mass flow rate at the terminal-velocity stage is a quarter of that at the initial stage, governed by both the decreasing in V_f and Y_f in Figs. (3b-c).

3. Results and discussions

Since the dripping flame is attached to a fuel drip that moves fast (~ 4 m/s) with a short lifetime (~ 1 s), there is difficulty in experimentally measuring the flame temperature or velocity field for model verification. Thus, two dripping-related variables measured in our previous experiment [1] are used to verify the model: 1) the dripping flame shedding frequency, and 2) the dripping extinction time. Comparisons between the simulations and experiments will be given when analyzing the modeled data.

2.5. Critical conditions for flame shedding

A non-reactive base case, i.e., a 2-mm spherical drip falling at a constant terminal velocity of 4 m/s, is first simulated without the flame chemistry. Without the gravity-induced acceleration, the entire sphere adopts a pure Stefan fuel flow of 0.92 mg/s at 400 °C, in the absence of any acceleration-introduced fuel injection (V_f = 0 m/s). Figure 4(a) shows the temperature contour (°C) of the base case after the flow is stabilized. As expected, a classical non-reactive von Kármán vortex street is observed under a shedding frequency of 615 Hz.

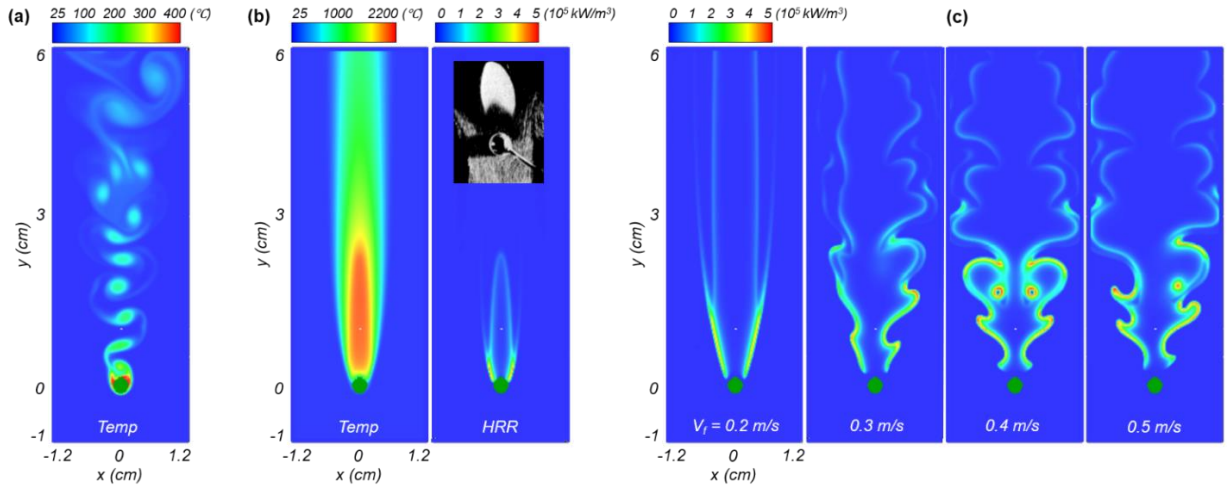

Fig. 4. (a) Non-reactive base case for 2-mm drip under the upward airflow of 4 m/s (Video S4), (b) reactive base with finite-rate flame chemistry (Video S5), compared with the wake flame in [19], and (c) flame shape varying with fuel injection velocity (Video S6).

Another reactive base case with the same drip size, upward airflow, and fuel mass flux is also simulated, where the 1-step infinite-rate flame chemistry and igniter are both included. Figure 4(b) shows the temperature (°C) and heat release rate (HRR, kW/m^3) contours for this reactive base. Different from the non-reactive one in Fig. 4(a), the vortex street does not occur with flame. Instead, a stable diffusion flame is observed in the wake region, which essentially reproduces the past experiment of a porous spherical gas burner in the constant upward flow [19, 20]. Further increasing the bottom airflow (V_a) will reduce the flame width, and eventually, blow-off occurs at V_a = 0.8 m/s, but the flame shedding never occurs, showing similarity to the experiments in [19, 20].

Then, the accelerated fall is simulated over a wide range of fuel injection velocities (V_f = 0.2 ~ 0.5 m/s). Figure 4(c) shows the instantaneous flame structure represented by the contour of HRR. At a small fuel injection velocity of V_f = 0.2 m/s, a stable and laminar wake flame is observed, which is essentially a classical Burke-Schumann diffusion flame, and it is similar to the base case in Fig. 4(b) except for a long tail. As V_f increases to 0.3 m/s, enhanced vortex structure can be observed with fluctuations propagating in the streamwise direction, indicating the occurrence of *flame shedding*. In other words, there is a lower threshold of $V_f \approx 0.25$ m/s for triggering flame shedding on a 2-mm drip. Further increasing V_f to 0.5 m/s, the process of flame shedding persists and becomes more stable, agreeing with experimental observation in Fig. 1(c) and Videos S3.

Figure 5 summarized the critical values of V_f for triggering the flame shedding under different drip sizes. For a fair comparison and a generalized discussion, the V_a used here behaves in the same law as Fig. 3(a), and a characteristic length L_c = 1 m and a characteristic velocity V_c = 1 m/s are used for a non-dimensional analysis. As the drip size decreases, a larger fuel injection velocity (V_f or a larger drip acceleration) is required to form the flame shedding, which follows the feature of von Kármán vortices [30]. In other words, there is a reluctance for small drips to develop to the shedding structures. Thus, for small drips (D < 2 mm), the failure of initiating the flame shedding will affect the flame attachment to drip and invite extinction in the early stage of dripping, which was also observed in the experiment [1]. For tiny drips (D < 0.63 mm), they will float up by the flame-introduced buoyancy [1], so not modeled here.

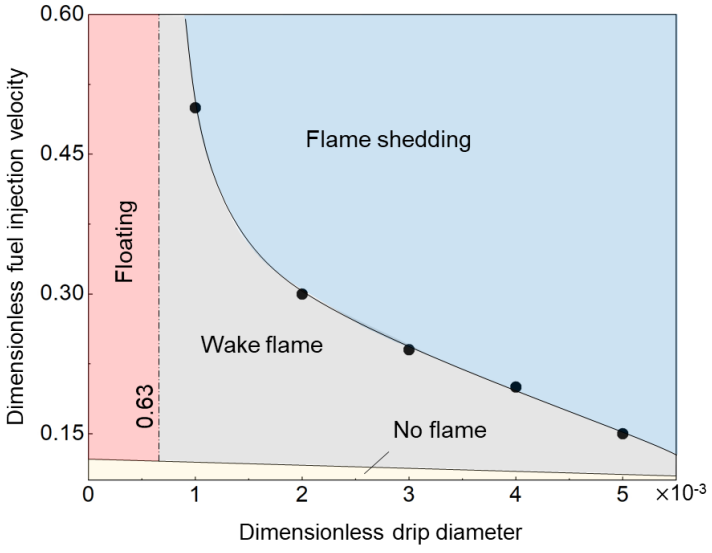

Fig. 5. Dependence of the minimum fuel injection velocity for triggering flame shedding on drip size.

3.1. Evolution of dripping structure

Figure 6 further shows the detailed evolution of the dripping flame from ignition to wake flame, and then to a lifted flame at the detaching moment, and eventually to the flame shedding, which gives a close agreement with the experimental observation. The modeling result confirms that the acceleration-induced fuel injection is a critical condition for forming stable flame shedding, despite a simplified 2-D model is adopted. Note that for a real 3-D spherical drip, the formation of vortex street should be easier than the 2-D case due to the vorticity dissipation in the additional dimension [33], which would occur under a lower critical *Re* number.

Figure 7 presents the modeled flame shedding frequencies of a 2-mm drip under different dripping velocities. To verify the model, the flame shedding frequencies obtained from dripping experiments [1] are also given. The characteristic parameters L_c = 1 m and V_c = 1 m/s are again used for non-dimensionalizing. Essentially, a good agreement between simulation and experiment is achieved. The slight discrepancy between the modeled and experimental frequencies can be attributed to the lack of one dimension in a 2-D configuration, which weakens the dissipations of vortices and leads to a higher frequency. It can be seen that the normal vortex shedding frequencies obtained by simulating non-reactive drips are also compared, which allows for concluding that the behavior of vortex shedding is more sensitive to the dripping velocity, rather than flame chemistry.

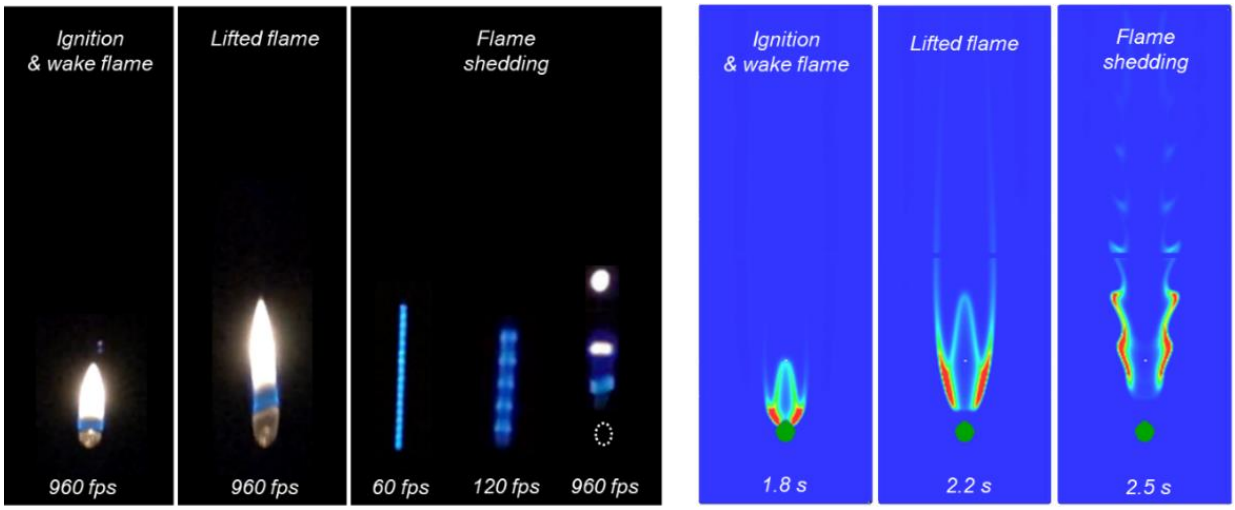

Fig. 6. The modeled evolution of dripping flame (Video S7) compared with the experiment.

3.2. Critical condition for dripping extinction

A typical flame extinction process of a 2-mm PE drip was shown in Fig. 8(a). During extinction, a stream of white smoke is continuously formed behind the drip and essentially follows the falling trajectory. This smoke is mainly the condensed fuel vapor (pyrolysis gases) from the drip, because little smoke is observed if the flame can attach to the drip. Thus, even though the cooling effect is strong during the fall, which could last for 0.9 s for a fall height of 2.6 m [1], the drip is still above the pyrolysis point to pyrolyze sufficient combustible gases. The top hemisphere, which receives more heating from the flame in the wake region, must be the critical zone for stabilizing the flame.

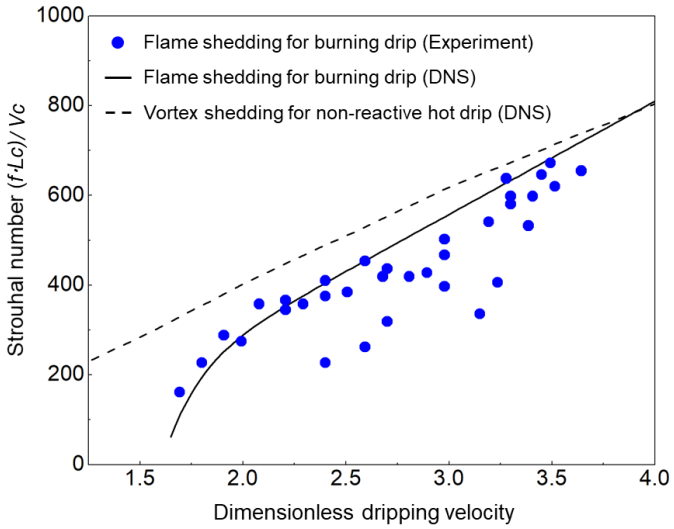

Fig. 7. Dimensionless dependence of flame shedding frequency on dripping velocity, where the vortex shedding frequency of non-reacting drip is also given.

Successfully modeling the flame shedding in Section 3.1 has paved the way for further investigating the extinction process of dripping flame. Figure 8(b) shows the modeled extinction process of a 2-mm drip, where the flame evolves in the same way as that observed in experiment within 60 ms before extinction. Here, the extinction boundary in Fig. 3(c-d) are applied after the moment of detachment (t = 2.1 s), that is, additional air is mixed into the fuel injection stream to mimic the air dilution in the real falling process (Fig. 3c), and the overall fuel mass flux is decreased to mimic the effect of air cooling (Fig. 3d). Note that in the absence of the shedding boundary (V_f), the model can only simulate the extinction process (or the blow-off) of a wake flame, similar to the past experiments in [19, 20], rather than the extinction of flame shedding.

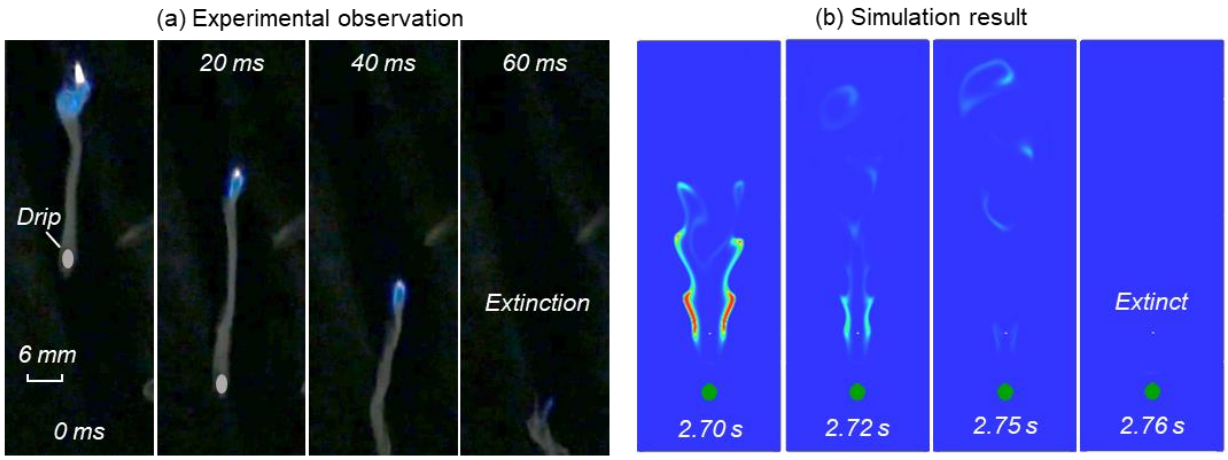

Fig. 8. (a) Snapshots of the extinction process of a 2-mm drip, and (b) modeled extinction process of dripping flame.

As the fuel mass fraction and flow continues to decrease from 2.1 to 2.7 s in Fig. 8(b), the flame-shedding process becomes weaker, but the flame can still be stabilized less than 5 mm above the drip and continue to heat the drip. It was noticed that if the polymer drip continues to release pure fuel gas, the flame shedding will persist indefinitely (Fig. 4c). After 2.7 s, flame shedding becomes destabilized

and moves upward until it reaches the up boundary of the monitored domain, i.e., extinction. Such a phenomenon was observed in the experiment (Fig. 8a), where the flame appears not able to catch up with the drip and the distance between flame and drip becomes larger. Also, the simulated extinction duration shows consistency with the experimental value.

To further explore the critical fuel boundary condition for triggering dripping extinction, both the shedding and extinction boundaries in Figs. 3(b-d) were varied in a large range, leading to an overall variation in the mass flux of fuel gas released by drip. Note that the bottom airflow (V_a or fall velocity) used here changes with the drip size following [1], so that the modeled results in Fig. 9(a) represent the response of drip behavior to the variation of fuel flux by drip at different drip sizes. Also, a characteristic mass flux of 1 g/m^2-s is used for a dimensionless discussion. If the fuel mass flux released from the drip is too low, the initial ignition will not be achieved. Therefore, an ignition threshold of fuel mass flux can be first identified, below which the flame cannot be self-sustained after removing the igniter.

Increasing the fuel mass flux above the ignition limit, the flame shedding will first be initiated in a lower fall velocity (V_a), but eventually, the extinction of flame shedding occurs during the fall under the extinction boundary conditions. Further increasing the fuel mass flux, a stable flame shedding will be achieved even when the drip reaches its terminal falling velocity, which is consistent with the experiment [1]. Accordingly, there is another extinction threshold for drip to carry the shedding structure stably, as also summarized in Fig. 9(a). Moreover, it is found that the increase in drip size leads to a reduction of ignition threshold. In other words, for larger drip, not only is it easier to ignite the fuel stream behind, but the flame shedding behind is more stable during the fall, which successfully explains why in experiment, the flame extinction always occurs when the drip size is smaller than 1.8 mm, and the probability of stable flame shedding increases to 70% as drip size increases to 2.6 mm [1].

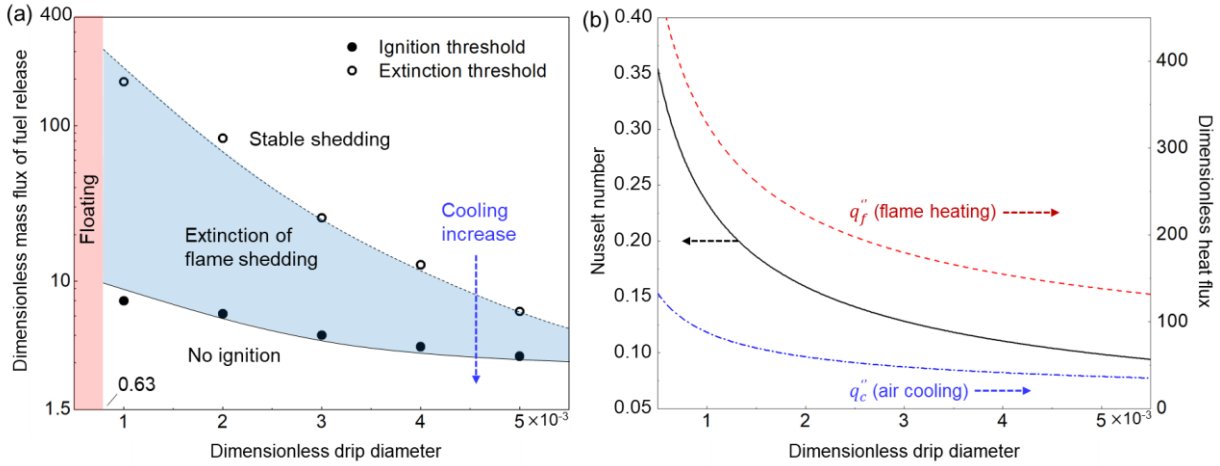

Fig. 9. (a) Dependence of the critical fuel mass flux for triggering dripping extinction on the drip size, and (b) dependence of Nusselt number, air cooling, and flame heating on the drip size at the terminal dripping stage.

In the early stage of dripping, when the flame is still close to the drip, the environmental cooling should not be the major factor for early extinction. Thus, the early-stage flame extinction is attributed to a failed formation of flame shedding where the flame cannot catch up with the drip, rather than the cooling. The cooling of airflow should be more important in the later fast-moving dripping stage. Figure 9(b) shows the modeled Nusselt number [34], air cooling, and flame heating as a function of drip size when the drip falls with the maximum terminal velocity. All data are non-dimensionalized by a

characteristic conduction coefficient 1 kW/m-k and a characteristic heat flux 1 kW/m^2. The inverse correlation between the convection coefficient and drip size indicates a faster heat transfer for smaller drip, which supports the above argument. Nevertheless, the convective heating of flame also increases with the decreasing drip diameter that effectively compensates the cooling of air, which partially explains why the dripping flame is quite stable for large drips, as long as a flame shedding structure is initiated. Note that to fully simulate the effect of air cooling and flame heating, the temperature and the finite-rate pyrolysis of drip should be included, which will be performed in future work.

4. Conclusions

In this work, the dripping flame was simulated by the DNS solver and 1-step finite-rate chemistry in FDS. Modeling results successfully reproduce the entire process of ignition, wake flame, and flame shedding, despite only a 2-D model is used. Analysis reveals that the gravity acceleration of drip initiates a fuel jet to form a lifted flame, which plays a critical role in the formation of flame shedding. Fundamentally, the flame shedding (or the observed blue-chain flame) is a combination of lifted flame and vortex street. For large drips, the flame shedding can be more easily initiated with a lower acceleration-introduced fuel injection velocity.

Modeling also reproduces the dripping extinction process caused by the dilution and cooling of air. As the diameter of the drip decreases, the dripping flame becomes more difficult to stabilize the shedding structure in the wake region, and the environmental cooling also increases to promote flame extinction, agreeing with the experimental observation. This work reveals the underlying mechanism of stabilizing the dripping flame and helps evaluate the risk and hazard of fire dripping phenomena. Future work should be conducted in more sophisticated numerical model with the finite-rate pyrolysis chemistry to quantify the real-time temperature evolution and pyrolysis rate of drip.

Acknowledgements

This work was supported by the National Natural Science Foundation of China (No. 52006185) and Hong Kong Polytechnic University (BE04). The authors thank Peiyi Sun and Yanhui Liu (HK PolyU) for assisting the data and imaging processes.

Compliance with Ethical Standards

Conflict of interest: The authors declare that they have no conflict of interests.

References

1. Huang, X.: Critical Drip Size and Blue Flame Shedding of Dripping Ignition in Fire. Scientific Reports. 8, 16528 (2018). https://doi.org/10.1038/s41598-018-34620-3
2. Kim, Y., Hossain, A., Nakamura, Y.: Numerical modeling of melting and dripping process of polymeric material subjected to moving heat flux: Prediction of drop time. Proceedings of the Combustion Institute. 35, 2555–2562 (2015). https://doi.org/10.1016/j.proci.2014.05.068
3. Lim, S.J., Kim, M., Park, J., Fujita, O., Chung, S.: Flame spread over electrical wire with AC electric fields: Internal circulation, fuel vapor-jet, spread rate acceleration, and molten insulator dripping. Combustion and Flame. 162, 1167–1175 (2015). https://doi.org/10.1016/j.combustflame.2014.10.009
4. Fang, J., Zhang, Y., Huang, X., Xue, Y., Wang, J., Zhao, S., He, X., Zhao, L.: Dripping and Fire Extinction Limits of Thin Wire: Effect of Pressure and Oxygen. Combustion Science and Technology. 193, 437–452 (2021). https://doi.org/10.1080/00102202.2019.1658578

5. Kobayashi, Y., Huang, X., Nakaya, S., Tsue, M., Fernandez-Pello, C.: Flame spread over horizontal and vertical wires: The role of dripping and core. Fire Safety Journal. 91, 112–122 (2017). https://doi.org/10.1016/j.firesaf.2017.03.047
6. Xie, Q., Tu, R., Wang, N., Ma, X., Jiang, X.: Experimental study on flowing burning behaviors of a pool fire with dripping of melted thermoplastics. Journal of Hazardous Materials. 267, 48–54 (2014). https://doi.org/10.1016/j.jhazmat.2013.12.033
7. McKenna, S.T., Jones, N., Peck, G., Dickens, K., Pawelec, W., Oradei, S., Harris, S., Stec, A.A., Hull, T.R.: Fire behaviour of modern façade materials – Understanding the Grenfell Tower fire. Journal of Hazardous Materials. 368, 115–123 (2019). https://doi.org/10.1016/j.jhazmat.2018.12.077
8. Wang, Y., Zhang, J.: Thermal stabilities of drops of burning thermoplastics under the UL 94 vertical test conditions. Journal of Hazardous Materials. 246–247, 103–109 (2013). https://doi.org/10.1016/j.jhazmat.2012.12.020
9. Xiong, C., Liu, Y., Xu, C., Huang, X.: Extinguishing the dripping flame by acoustic wave. Fire Safety Journal. 103109 (2020). https://doi.org/10.1016/j.firesaf.2020.103109
10. Wang, Y., Kang, W., Zhang, X., Chen, C., Sun, P., Zhang, F., Li, S.: Development of a pendant experiment using melt indexer for correlation with the large-size dripping in the UL-94 test. Fire and Materials. 42, 436–446 (2018). https://doi.org/10.1002/fam.2510
11. He, H., Zhang, Q., Tu, R., Zhao, L., Liu, J., Zhang, Y.: Molten thermoplastic dripping behavior induced by flame spread over wire insulation under overload currents. Journal of Hazardous Materials. 320, 628–634 (2016). https://doi.org/10.1016/j.jhazmat.2016.07.070
12. Kobayashi, Y., Konno, Y., Huang, X., Nakaya, S., Tsue, M., Hashimoto, N., Fujita, O., Fernandez-Pello, C.: Effect of insulation melting and dripping on opposed flame spread over laboratory simulated electrical wires. Fire Safety Journal. 95, 1–10 (2018). https://doi.org/10.1016/j.firesaf.2017.10.006
13. Sun, P., Lin, S., Huang, X.: Ignition of thin fuel by thermoplastic drips: An experimental study for the dripping ignition theory. Fire Safety Journal. 115, 103006 (2020). https://doi.org/10.1016/j.firesaf.2020.103006
14. Miyamoto, K., Huang, X., Hashimoto, N., Fujita, O., Fernandez-Pello, C.: Limiting oxygen concentration (LOC) of burning polyethylene insulated wires under external radiation. Fire Safety Journal. 86, 32–40 (2016). https://doi.org/10.1016/j.firesaf.2016.09.004
15. Meinier, R., Sonnier, R., Zavaleta, P., Suard, S., Ferry, L.: Fire behavior of halogen-free flame retardant electrical cables with the cone calorimeter. Journal of Hazardous Materials. 342, 306–316 (2018). https://doi.org/10.1016/j.jhazmat.2017.08.027
16. Takahashi, S., Takeuchi, H., Ito, H., Nakamura, Y., Fujita, O.: Study on unsteady molten insulation volume change during flame spreading over wire insulation in microgravity. Proceedings of the Combustion Institute. 34, 2657–2664 (2013). https://doi.org/10.1016/j.proci.2012.06.158
17. Onate, E., Rossi, R., Idelsohn, S.R., Butler, K.M.: Comparison of Linear and Classical Velocity Update Rules in Particle Swarm Optimisation: Notes on Diversity. International Journal for Numerical Methods in Engineering. 2006 (2006). https://doi.org/10.1002/nme
18. Kim, Y., Hossain, A., Nakamura, Y.: Numerical study of melting of a phase change material (PCM) enhanced by deformation of a liquid-gas interface. International Journal of Heat and Mass Transfer. 63, 101–112 (2013). https://doi.org/10.1016/j.ijheatmasstransfer.2013.03.052
19. Gollahalli, S.R., Brzustowski, T.A.: Experimental studies on the flame structure in the wake of a burning droplet. Symposium (International) on Combustion. 14, 1333–1344 (1973). https://doi.org/10.1016/S0082-0784(73)80119-5
20. Raghavan, V., Babu, V., Sundararajan, T., Natarajan, R.: Flame shapes and burning rates of spherical fuel particles in a mixed convective environment. International Journal of Heat and Mass Transfer. 48, 5354–5370 (2005). https://doi.org/10.1016/j.ijheatmasstransfer.2005.07.029
21. Cavaliere, D.E., Kariuki, J., Mastorakos, E.: A comparison of the blow-off behaviour of swirl-stabilized premixed, non-premixed and spray flames. Flow, Turbulence and Combustion. 91, 347–372 (2013). https://doi.org/10.1007/s10494-013-9470-z
22. Kariuki, J., Dowlut, A., Balachandran, R., Mastorakos, E.: Heat Release Imaging in Turbulent

Premixed Ethylene-Air Flames Near Blow-off. Flow, Turbulence and Combustion. 96, 1039–1051 (2016). https://doi.org/10.1007/s10494-016-9720-y
23. Fereres, S., Lautenberger, C., Fernandez-Pello, A.C., Urban, D.L., Ruff, G.A.: Understanding ambient pressure effects on piloted ignition through numerical modeling. Combustion and Flame. 159, 3544–3553 (2012). https://doi.org/10.1016/j.combustflame.2012.08.006
24. Navarro-Martinez, S., Kronenburg, A.: Flame stabilization mechanisms in lifted flames. Flow, Turbulence and Combustion. 87, 377–406 (2011). https://doi.org/10.1007/s10494-010-9320-1
25. Lyons, K.M.: Toward an understanding of the stabilization mechanisms of lifted turbulent jet flames: Experiments. Progress in Energy and Combustion Science. 33, 211–231 (2007). https://doi.org/10.1016/j.pecs.2006.11.001
26. Mcgrattan, K., Hostikka, S., Mcdermott, R., Floyd, J., Weinschenk, C., Overholt, K.: "Fire Dynamics Simulator User's Guide", NIST Special Publication 1019 6th Ed. National Institute of Standards and Technology, MA. (2013)
27. Geikie, M.K., Carr, Z.R., A. Ahmed, K., Forliti, D.J.: On the Flame-generated Vorticity Dynamics of Bluff-body-stabilized Premixed Flames. Flow, Turbulence and Combustion. 99, 487–509 (2017). https://doi.org/10.1007/s10494-017-9822-1
28. Li, G., Naud, B., Roekaerts, D.: Numerical Investigation of a Bluff-Body Stabilised Nonpremixed Flame with Differential Reynolds-Stress Models. Flow, Turbulence and Combustion. 70, 211–240 (2003). https://doi.org/10.1023/B:APPL.0000004931.07292.55
29. Morales, A.J., Lasky, I.M., Geikie, M.K., Engelmann, C.A., Ahmed, K.A.: Mechanisms of flame extinction and lean blowout of bluff body stabilized flames. Combustion and Flame. 203, 31–45 (2019). https://doi.org/10.1016/j.combustflame.2019.02.002
30. Sallet, D.W.: On the Spacing of Karman Vortices. Journal of Applied Mechanics. 36, 370–372 (1969)
31. Migita, T., Yamahata, T., Strempfl, P., Matsuoka, T., Nakamura, Y.: Methodology to Achieve Pseudo 1-D Combustion System of Polymeric Materials Using Low-Pressured Technique. Fire Technology. (2020). https://doi.org/10.1007/s10694-019-00877-x
32. Sun, P., Wu, C., Zhu, F., Wang, S., Huang, X.: Microgravity combustion of polyethylene droplet in drop tower. Combustion and Flame. 222, 18–26 (2020). https://doi.org/10.1016/j.combustflame.2020.08.032
33. Attili, A., Bisetti, F.: Statistics of Scalar Dissipation and Strain/Vorticity/Scalar Gradient Alignment in Turbulent Nonpremixed Jet Flames. Flow, Turbulence and Combustion. 103, 625–642 (2019). https://doi.org/10.1007/s10494-019-00044-w
34. Drysdale, D.: An Introduction to Fire Dynamics. John Wiley & Sons, Ltd, Chichester, UK (2011)

Appendix

Given that $\eta = L_k/D$, a cylinder bluff body flow [30] follows:

$$S_t^2\eta^3 + 0.529S_t\eta^2 - 1.528\eta + 1.592\left(C_D - \frac{4}{\sqrt{Re}}\right) = 0 \qquad (A1)$$

where L_k is the distance between two successive vortices of the vortex street, D is the drip diameter, S_t is the Strouhal number and C_D is the drag coefficient. For the current regime, S_t = 0.21 and C_D = 1.05 [30]. As D changes from 1 to 5 mm, the Reynolds number $Re = V_{at} \cdot D/v$, where V_{at} denotes the maximum airflow velocity and v = 15.89×10^{-6} N·s/m^2 is the kinetic viscosity of air at 300 K, varies from 252 to 1260. Thus, the fuel injection velocities $V_f \approx a\Delta t = \sqrt{2gL_k}$ are 0.28, 0.4, 0.49, 0.56 and 0.63 m/s, respectively.